Chapter 9
Application of Bioluminescence Imaging (BLI) to the Study of the Animal Models of Human Infectious Diseases

Hana Golding and Marina Zaitseva

Abstract Traditional approaches in measuring the efficacy of antimicrobials, antivirals, antifungals, and antiparasitic therapies have limitations which contribute to noise in efficacy assessment. These include the following: (1) large number of animals must be sacrificed at multiple time points to assess the effects of therapy on pathogen titers in the organs; (2) weight loss of 25–30 % in animals requires ethical animal euthanasia which may be unscheduled and skew sampling; and (3) the organ titers are based upon ex vivo culture or analysis. Such limitations can lead to erroneous conclusions regarding drug efficacy versus spontaneous recovery. One needs to evaluate dissemination of the pathogen in vivo within the same animal to truly measure efficacy. Bioluminescence imaging (BLI) has been developed as a new method to monitor infections in small animal models. BLI is based on noninvasive measurement of biomarkers possessing a light-producing luciferin or other light-emitting metabolic substrates. This imaging platform is now a widely used technique in oncology, tumor metastasis, establishing efficacy of anticancer and anti-infective therapies, detecting protein–protein interactions, detecting transgene expression in vivo, and many more. BLI, importantly, enables each animal to be used as its own control over time, thus limiting the number of animals required in studies and minimizing animal-to-animal variations which improves statistical precision of efficacy outcomes. In this chapter we describe applications of BLI in the study of infection, reveal important limitations of the technique, and summarize recent work in murine microbial and viral models.

This book chapter reflects the views of the authors and should not be construed to represent FDA's views or policies.

H. Golding, Ph.D. • M. Zaitseva (✉)
Division of Viral Products (DVP), Center for Biologics Evaluation and Research (CBER), Food and Drug Administration (FDA), Bethesda, MD, USA
e-mail: marina.zaitseva@fda.hhs.gov

B.R. Moyer et al. (eds.), *Pharmaco-Imaging in Drug and Biologics Development*, AAPS Advances in the Pharmaceutical Sciences Series 8, DOI 10.1007/978-1-4614-8247-5_9,

9.1 Brief Description of the BLI Principles and Methodology of the Experiments Utilizing BLI as a Tool to Study Infections in Mice

9.1.1 Tissue Optics

The optical properties of the tissue to a large degree determine the sensitivity of deep-tissue imaging that utilizes fluorescent or bioluminescent probes. For example wavelengths of less than 600 nm are strongly quenched by hemoglobin molecule, while water absorption quenches wavelengths above 900 nm. In addition, endogenous chromophores such as elastin, collagen, tryptophan, NADH, porphyrins, and flavins in animal tissues and in the skin are subjected to autofluorescence upon excitation in wavelengths below 600 nm. Therefore, although fluorescent signals are generally brighter than bioluminescent signals, the very low autoluminescent levels usually result in superior signal-to-background ratios for bioluminescent imaging, particularly compared with fluorescent imaging in the green to red part of the spectrum (Lin et al. 2009; Troy et al. 2004). Based upon this fundamental differences in the signal-to-noise ratio, bioluminescent reporters remain to date more sensitive than fluorescent reporters for deep-tissue imaging applications.

9.1.2 Luciferases

Production of visible light is a natural phenomenon observed in some marine and terrestrial species. The mechanism responsible for light production is similar between these organisms and involves oxidation of an aldehyde substrate which is catalyzed by the enzyme luciferase. The major differences in the produced light between species are based on the source of the substrate, and on the kinetics and wavelength of the emitted light.

Genomes of bacteria such as Gram-negative bacteria *Photorhabdus luminescen*s and *Xenorhabdus luminescens* contain *lux* operon that encodes genes to synthesize luciferase and substrate luciferin, thus omitting the need to provide the substrate exogenously. Bacteria expressing the *lux* operon constitutively produce light with a peak emission at 490 nm. *Lux* operon has been widely used for bioluminescence imaging (BLI) of bacterial infections.

The luciferase enzymes from the North American firefly (Fluc) (*Photinus pyralis*) and from click beetle (*Pyrophorus plagiophthalamus*) are most widely used for BLI. These enzymes are monomeric proteins encoded by a single gene (*luc*). Modified firefly luciferase is expressed in the cytoplasm with a half-life of about 3 h. Luciferase catalyzes chemical reaction where exogenously provided D-luciferin substrate is oxidized in the presence of ATP-Mg^{+2} and O_2-generating oxyluciferin, CO_2, AMP, and light with a broad spectral emission that peaks at 560 nm but that

also includes a significant fraction of light above 600 nm (Gould and Subramani 1988). The luciferase enzymes from click beetle have been optimized to produce green-orange (544 nm) or red (611 nm) light after oxidizing luciferin. The longer wavelength light in the orange-red spectrum exhibits better penetration in living tissue and is therefore optimally suited for use in whole-animal imaging modality. The currently available methods allow detection of $>2.4 \times 10^5$ molecules of luciferase (Gould and Subramani 1988). The firefly luciferase is an oxygen scavenger. Due to the high homology to endogenous enzymes in mammalian cells, firefly luciferase is poorly immunogenic.

D-Luciferin substrate is a small molecule which penetrates across cell membranes and the blood–brain barrier. The mechanism of cellular uptake of luciferin is not fully elucidated and the role of specific membrane transporters in inward delivery and efflux of luciferin has been recently suggested (Zhang et al. 2012). Following injection of the substrate via intraperitoneal (IP) route, signal peaks around 15 min followed by a plateau phase of 15–20 min after which it steadily declines (Paroo et al. 2004). Studies that used radiolabeled D-luciferin showed that the kinetics of uptake and biodistribution varied significantly depending on the route of administration (Berger et al. 2008; Lee et al. 2003). The D-luciferin is not metabolized and is excreted via the kidneys within 2 h post injection.

Luciferase from marine organisms, *Renilla* (sea pansy) and *Gaussia* (copopod) luciferases, utilize coelenterazine substrate to produce light with emission peak at approximately 480 nm. The availability and in vivo distribution of the coelenterazine substrate is more limited than of the D-luciferin and therefore the coelentrazine may not be easily available for cells infected with *Renilla* luciferase-expressing pathogens. Bioluminescence from *Renilla* luciferase differs in kinetics from firefly luciferase peaking in about 1 min followed by decline in 10 min after i.v. injection (Paroo et al. 2004).

9.1.3 Detection and Measurement of Bioluminescence In Vivo in Live Animals

First bioimaging experiments utilizing photonic detection of light-emitting bacteria were performed in mice infected with luciferase-expressing *Salmonella typhimurium* (Contag et al. 1995). The same study also compared the sensitivity of bioluminescence measurements performed in live animals and in extracted organs and determined a five- to tenfold reduction in luminescence per cm of tissue, thus setting up the limitations for imaging of organs that are located deep in the body. The advancement in detector technologies greatly increased the sensitivity of charge-coupled device (CCD) cameras that can be cooled to −120 °C to maximally suppress dark current/noise allowing detection of minute amounts of bioluminescent light. As mammalian tissues are mainly absorbing in the blue, green, and yellow regions, the cooled CCD cameras are designed to detect red and near-red light (Contag and Bachmann 2002).

In a typical experiment, mice are infected with luciferase-expressing pathogen, receive a single dose of a luciferin substrate (the substrate is not injected when bacteria expressing *lux* operon are used), and are imaged while under anesthesia. Light emitted by infected organ(s) is captured by a CCD device during preset exposure time, is converted to numerical values using specific software, and is displayed on the monitor in pseudotyped colors scaled to reflect intensity of the captured light. During analysis of recorded images, the areas in the image that exhibit color are marked as regions of interest (ROIs) and the amount of light within designated ROIs is quantified as photon fluxes. Often, to adjust for various exposure times and sizes of ROIs, fluxes are normalized per unit of time and per area and are expressed as flux/s/cm^2. While normalization provides some advantage for comparison of luminescence signals between groups, one needs to remember that measured bioluminescence is relative and comparisons cannot be applied to tissues that are located at various depths of the organism. Therefore, in most studies, a set of ROIs is established for each site/organ, and groups of mice are compared and followed using the same ROIs throughout the study. Once these limitations are taken into consideration, it can be expected that BLI can measure luminescence signals in vivo with high sensitivity and reproducibility. The emitted fluxes can be used as quantitative measurements for statistical analyses. However, the correlation between bioluminescence and viral loads needs to be established for each organism/infection model.

Early studies using cell lines stably expressing luciferase showed that BLI can detect as few as approximately 30 cells in vitro and 1×10^3 cells in a mouse (Sweeney et al. 1999). However, it is important to note that the strength of promoters used to drive luciferase expression in recombinant viruses or bacteria may affect limits of detection. Therefore, it is essential to generate correlation curves for each luciferase-expressing pathogen used in the study. Our own data as well as reports published by other investigators have shown that measurements of photon fluxes emitted by recombinant viruses expressing luciferase correlated in linear fashion with viral loads measured in organs isolated from infected mice, thus supporting the notion that bioluminescence provides a direct measure of in-host viral replication and dissemination (Cook and Griffin 2003; Luker et al. 2002; Luker and Luker 2008; Zaitseva et al. 2009). It is also important to note that because luciferase requires ATP for generating light from luciferin, the IVIS system measures luciferase activity only in cells. Luciferase in the plasma is not measured and any signal acquired is from the organ not the blood.

9.2 BLI for Monitoring Viral Infections

The introduction of the luciferase gene into the genome of vaccinia virus (VACV) was the first attempt to use measurements of emitted light as an alternative approach to traditional plaque assay to quantify DNA viruses (Rodriguez et al. 1988). At a high infection rate, recombinant VACV produces about 10,000 particles per cell, which contributes to the 1,000-fold higher sensitivity in detecting VACV in vitro by

measuring luciferase activity compared with β-galactosidase as reporter-gene system (Rodriguez et al. 1988). Several studies used luciferase-expressing VACV to assess viral–host interactions. BLI of IFNα receptor knockout (KO) or TLR4 knockout mice infected with VACV-reporter virus showed that mutant mice had increased dissemination and higher levels of bioluminescence signal in internal organs that correlated with lower survival rates (Hutchens et al. 2008; Luker et al. 2005). More severe pathogenesis was observed in the TLR4 KO mice, and was attributed to increased lung inflammation. It suggested that innate immune receptors play a major role in limiting in-host dissemination of VACV (Hutchens et al. 2008). In our laboratory, BLI was extensively used to evaluate effects of anti-smallpox vaccine and antiviral treatments on dissemination of two strains of recombinant VACV expressing luciferase, WRvFire, and IHD-J-Luc, and the results of these studies are summarized at the end of this chapter (Zaitseva et al. 2009, 2011).

In vivo dissemination of a herpes simplex virus type I (HSV-1) was monitored using a recombinant strain of KOS HSV-1 virus that encoded both *firefly* luciferase and *Renilla* luciferase under the control of an early gene promoter (Luker et al. 2002). The validity of this model to study HSV-1 pathogenesis was confirmed by showing that valacyclovir, a potent inhibitor of HSV-1 replication, reduced bioluminescence in the eyes of mice in vivo and reduced viral titers in the tear film material ex vivo following KOS HSV-1 infection via corneal scarification. The same study also pointed to several limitations of the BLI; the activity of *Renilla* luciferase could be detected only after direct inoculation of the substrate (coelenterazine) in infected eyes but not after systemic administration. In addition, due to low spatial resolution of the 2-D imaging system, bioluminescence from the site of infection in the cornea could not be separated from the subsequent spread of infection to the periocular tissues (Luker et al. 2002). In the follow-up studies, BLI was used to study the role of IFNα in protection from HSV-1 infection using mice lacking IFNα R1 and mice lacking TLR9 and MyD88, known inducers of IFNα (Krug et al. 2004; Luker et al. 2003). IFNα R1 KO mice infected with reporter virus exhibited higher bioluminescence in internal organs compared with wild-type mice confirming that dissemination of HSV-1 was controlled by IFNα (Luker et al. 2003). In contrast, luminescence was not increased in mice lacking TLR9 or MyD88 suggesting that TLR9/MyD88 pathway was not involved in controlling viral replication in vivo (Krug et al. 2004).

While large DNA viruses such as poxviruses and HSV virus allow for insertion of a large portion of foreign DNA, the insertion of a reporter gene in RNA viruses is more challenging. Nevertheless, several laboratories reported successful construction of recombinant RNA viruses expressing luciferase and development of animal models where infection with recombinant RNA viruses was monitored by BLI.

Dengue virus (DENV) is a global disease threat for which there are no approved antivirals or vaccines. A recent report described an infectious recombinant *fluc-expressing* DENV that was sensitive to neutralizing antibodies and to antiviral agents, adenosine nucleoside NITD008 and mycophenolic acid in vitro (Schoggins et al. 2012). However, of the two compounds, only NITD008 but not mycophenolic acid suppressed virus replication in vivo, thus demonstrating that BLI may be a

useful drug discovery tool to identify compounds that target DENV in vivo (Schoggins et al. 2012).

BLI was used to study infections of mice with two members of the family of alphaviruses, Venezuelan equine encephalitis virus (VEEV) and Sindbis virus (SV), that are an important cause of encephalitis in the Americas, causing disease in horses, birds, and humans. Following intranasal infection of mice with TC83-luciferase, a highly attenuated strain of VEEV that replicates in mouse brain, bioluminescence was detected in the CNS at least 3 days before the onset of clinical signs of disease, including encephalitis and meningitis, thus allowing humane treatment of animals (Patterson et al. 2011). Moreover, this model was successfully utilized to show that human antiviral drug and TLR3 agonist Ampligen effectively inhibited viral dissemination after intraperitoneal but not intranasal delivery (Patterson et al. 2011). In the SV infection model, BLI enabled authors to visualize invasion of CNS by TRNSV-Luc recombinant SV from peripheral sites of viral replication following subcutaneous (s.c.) inoculation (Cook and Griffin 2003). Replication of SV was detected in the noses of mice at day 1 post infections followed by lower spinal cords and brains, thus providing evidence for the previously suggested nasal neuroepithelium as the initial site for replication of the SV prior to entering of the CNS (Cook and Griffin 2003).

An interesting application for BLI was recently reported in infection of mice with highly contagious respiratory parainfluenza virus (PIV) as a surrogate model for transmission of respiratory syncytial virus (RSV) in humans (Burke et al. 2011). Here authors utilized BLI to follow animal-to-animal transmission of a negative-RNA strand recombinant rSeV-luc(M-F*) virus that was phenotypically similar to wild-type Sendai virus (Burke et al. 2011). The study revealed important differences in the role of viral replication in pathogenesis versus transmission: infection of the upper respiratory tract and trachea were associated with animal-to-animal transmission while infection in the lungs was associated with pathogenesis (weight loss and mortality) (Burke et al. 2011).

9.3 BLI for In Vivo Monitoring of Bacterial Infections and Antibacterial Treatments

Bacterial *lux* operon contains genes coding for both luciferase and its substrate, and therefore BLI of bacterial infections in animal models does not require injections of the substrate. Yet, creating Gram-positive bioluminescent bacteria is complicated due to inability of the ribosomes in Gram-positive (G+) bacteria to bind and translate mRNA of the *lux* operon from Gram-negative *Photorhabdus luminescens*. Therefore two approaches were developed to adapt G+ bacteria for BLI. The G+ ribosome-binding sites were installed above each gene of the *P. luminescens lux* operon and the created cassette was inserted into the chromosome of G+ bacteria; this technique was implemented in animal models of infections with *Staphylococcus aureus* and *Streptococcus pneumoniae* (Francis et al. 2000, 2001; Kadurugamuwa et al. 2003;

Xiong et al. 2005). In other studies, *lux* operon was provided within the reporter plasmids to follow replication and dissemination of *S. aureus, Yersinia pestis*, and *Francisella tularensis* (Bernthal et al. 2010; Bina et al. 2010; Nham et al. 2012; Sha et al. 2013).

The antimicrobial effects of several antibiotics were evaluated by BLI in the mouse and in the rat models of *S. aureus* bacterial biofilm infections, commonly associated with implantation of prosthetic devices in humans and with *S. aureus* endocarditis (Kadurugamuwa et al. 2003; Xiong et al. 2005). In the first study, catheter colonized with luminescent *S. aureus* XEN 29 was implanted s.c. in mice. Bacterial growth and sensitivity to rifampin but not tobramycin or ciprofloxacin were determined by BLI and were confirmed by colony counts in extracted catheters ex vivo. Importantly, after the rifampin was discontinued, the rebound of the signal was observed, and was mediated by growth of the rifampin-resistant staphylococci (Kadurugamuwa et al. 2003). In the rat model of aortic infective endocarditis (IE), the effects of several anti-staphylococcal agents on *S. aureus* XEN 29 bacterial burden in cardiac vegetations were monitored by BLI. Microbial relapse due to discontinuation of vancomycin therapy was correctly predicted based on increased cardiac bioluminescence (Xiong et al. 2005). In addition, bioluminescent SH1000 *S. aureus* strain containing the *lux* genes within a plasmid was used to evaluate effectiveness of antibiotic treatment in a model of post-arthroplasty *S. aureus* joint infection in genetically engineered mice with fluorescent neutrophils (LysEGFP mice) (Bernthal et al. 2010). Following inoculation of the SH1000 *S. aureus* into the mouse joint containing orthopedic implant, increased bioluminescence, swelling of the affected leg, and increased EGFP-neutrophil fluorescence were observed. Importantly, bioluminescence and fluorescence were substantially lower in mice that received implants pre-coated with antibiotic-eluting polymers suggesting that bacterial biofilm and inflammatory responses could be prevented if sufficient concentrations of antibiotics are constitutively present at the surface of the implant (Bernthal et al. 2010).

The potential use of multidrug-resistant *Yersinia pestis* as a biological warfare and the reappearance of human plague in countries where no cases have been reported for decades renewed interest in the development of anti-*Y. pestis* drugs and vaccine. Virulent variants of *Y. pestis* C092 containing *lux* operon within pGEN-luxCDABE or within pUTmini-TN::luxKM2 reporter plasmids were recently generated and used in mouse models of bubonic plague and pneumonic plague, respectively (Nham et al. 2012; Sha et al. 2013). To mimic the natural route of transmission of bubonic plague in humans via flea bite, the bioluminescent *Y. pestits* C092 was inoculated into mice s.c. at *linea alba*. Using BLI, the in-host progression of the infection was monitored in real time. The data showed that after initial multiplication at the injection site, bacteria migrated from one lymph node to another via the lymphatic stream and once it reached the lymph nodes, the bacteria progressed very rapidly throughout the body (septicemic phase) leading to death within 2 days (Nham et al. 2012). In the mouse model of pneumonic plague, following intranasal inoculation, bioluminescent *Y. pestis* C092 established infection in the lungs prior to dissemination to the liver and spleen. Importantly, using this model, the authors

demonstrated that daily treatments with levofloxacin (10 mg/kg/day) starting 24 h post infection protected mice from lethality and completely reduced bioluminescence, indicating that this antimicrobial treatment killed bacteria early in the course of infection and prevented its dissemination (Sha et al. 2013).

Recently, BLI was employed in the mouse model of *E. coli*-induced infectious diarrhea (Rhee et al. 2011). In the first study, Enteropathogenic *E. coli* (EPEC) was transformed with *lux* operon-containing plasmid and used to localize intestinal sites where bacteria disseminate following oral administration. To allow for consistent EPEC colonization, mice were pretreated with streptomycin for 1 day prior to bacterial infection. In addition, because luciferase requires oxygen to induce bioluminescence, the entire intestine (duodenum–rectum) was excised, aerated, and subjected to BLI ex vivo. The study showed that cecum and colon, but not rectum, were the main sites of colonization by EPEC (Rhee et al. 2011). Human infections with EPEC are often studied using a genetically relevant murine *Citrobacter rodentium* which induces transmissible colitis and colonic epithelial cell hyperplasia in mice. A combination of a 2D BLI with a 3D diffuse light imaging tomography with μCT imaging (DLIT-μCT) (to determine the exact location of the BL foci in vivo) was employed for the first time to evaluate the effects of prophylactic treatment with *Bifidobacterium breve* UCC2003 probiotics on *C. rodentium* dissemination (Collins et al. 2012). The results showed that *C. rodentium* forms focal infection in the cecum, followed by colonization of the large intestine. Interestingly, pretreatment with *B. breve* did not prevent *C. rodentium* colonization, but significantly reduced distribution within the large intestine and ameliorated intestinal inflammation (as was confirmed by histological analysis of the lamina propria) (Collins et al. 2012).

9.4 BLI for In Vivo Monitoring of Infections with Parasites and Fungi

Recent reports demonstrated the utility of BLI in following infections of mice with parasites and fungi. The recombinant protozoan parasites *Leishmania donovani*, *Leishmania major*, and *Leishmania amazonensis* with genomic expression of firefly luciferase gene were shown to infect bone marrow-derived macrophages in vitro and to form lesions upon intradermal infection of mice in vivo (Lang et al. 2005; Roy et al. 2000). Importantly, light produced by in vitro-infected macrophages and light detected in lesions following in vivo infections correlated in linear fashion with the number of parasites measured by culture-based assay. In addition, the in vitro infection was shown to be useful for rapid screening of anti-Leishmania agents (Lang et al. 2005).

Interesting results were obtained with bioluminescent luciferase-expressing *Toxoplasma gondii* in the study of parasite reactivation after latency in chronically infected mice (Saeij et al. 2005). BLI of live mice showed that the parasites emerged in different anatomical sites: in the head and neck area in mice that were infected with highly virulent *T. gondii* and in the abdomen of mice infected with low-virulence *T. gondii*, thus linking virulence with anatomical location of the parasite (Saeij et al. 2005).

For visualization of *Candida albicans* fungal infections, clinical isolate of *Candida albicans* was stably transformed with a codon-optimized luciferase gene (Doyle et al. 2006). Chronic infections were established in mice and bioluminescence in vaginal tissue correlated with fungal loads assayed in vaginal lavage. Importantly, clearance of the infection following treatment with the antifungal drug, miconazole, as determined by imaging in vivo was confirmed in the ex vivo detection of fungal loads (Doyle et al. 2006). This study was further extended by expressing a synthetic version of the *Gaussia princeps* luciferase gene as part of the *C. albicans* GPI-linked cell wall protein (Enjalbert et al. 2009). In this construct, luciferase is expressed on cell surface and is readily accessible to the substrate irrespectively of whether the fungus is in the yeast or in the hyphal form, and thus omitting the problem of limited permeability of the hyphal cells for luciferin substrate (Enjalbert et al. 2009).

9.4.1 Conclusion

In conclusion, BLI of small rodents infected with pathogens engineered to express luciferase enzymes provides a useful tool to study pathogen–host interactions and for drug discovery and preclinical testing of therapies and vaccines. In all of these studies there are several issues that need to be taken into consideration while planning the experiments and interpreting the data. These factors include but are not limited to the following: susceptibility to the infection can be affected by genetics of the mouse strain, the intensity of the recorded signal is strongly affected by the color of the mouse fur and underlying skin, introduction of the luciferase gene may attenuate pathogenicity, and animal-to-animal variability in signal intensity and between anatomical sites.

It is important to also note that the improvements in gene sequences of luciferase enzymes and optimization of the expression techniques during the past several years dramatically expanded the panel of pathogens expressing luciferase reporter genes, enabling in vivo imaging during preclinical studies. As described above, some bioluminescent pathogens were already tested in prototype models for drug evaluation and others such as *Mycobacterium tuberculosis*, *Vibrio cholerae*, and *Bacillus anthracis* were already engineered for in vivo luminescence imaging and future studies will show their usefulness for preclinical studies of antibacterial treatments (Andreu et al. 2010; Glomski et al. 2007; Morin and Kaper 2009).

9.5 Bioimaging of Mice Infected with Recombinant Vaccinia Viruses Expressing Luciferase

Smallpox, a highly lethal disease with nearly 30 % mortality rate, is caused by infection with variola virus. Smallpox is highly contagious and is thought to be transmitted as an aerosol and via fomites, causing lung infection followed by viremic phase and development of classic disseminated rash or "pocks" (Fenner et al. 1988; Henderson et al. 1999).

Vaccination of the general public against smallpox was discontinued in the USA in 1972 after the massive worldwide vaccination campaign that eradicated smallpox. Yet the threat of potential release of variola virus as a bioterrorist agent and the emergence of monkeypox virus infections in humans have led to renewed interests in the development of antiviral drugs and safer vaccines (Henderson et al. 1999; Rimoin et al. 2010; Whitley 2003). The currently licensed smallpox vaccine containing replicating VACV (that belongs to the same family of orthopoxviruses as variola virus) poses a significant risk to individuals with certain skin disorders or immunodeficiency conditions (Baker et al. 2003; Belongia and Naleway 2003). To manage cases of vaccine-associated complications and for treatments of accidental exposures, new antiviral compounds are being investigated in animal models and in clinical trials in humans (Neyts and De Clercq 2003).

Preclinical testing of new anti-smallpox vaccines and therapeutics is performed using several animal models as surrogate models of variola virus infection in humans including infection of macaques with monkeypox virus (Edghill-Smith et al. 2005; Hooper et al. 2004; Panchanathan et al. 2007). However, due to the expense and requirement for Biosafety Level 3 facilities, nonhuman primate models cannot be widely used for smallpox vaccine development. The majority of preclinical testing and initial characterization of smallpox vaccines and therapies are performed with the Western Reserve (WR) strain of VACV or with ectromelia virus, which is highly lethal in mice. Various endpoints are used to follow infections in mice and include weight loss, pox lesion scoring, and viral load measurements by plaque formation on sensitive cell lines. These endpoints are not optimal as they cannot avoid morbidity or accurately predict lethality of individual animals. They require large number of animals in order to determine survival rates and to quantify viral loads in internal organs. Lethality was frequently used as an endpoint in the past, but is no longer acceptable.

To get an inside view on the pharmacology and mechanism of protection from lethality provided by vaccines against smallpox and antiviral therapies, our laboratory developed a complex approach where we employ bioluminescence to record dissemination and replication of VACV in live mice in the presence of antiviral treatments. In the experiments, mice are infected with a recombinant VACV which expresses firefly luciferase (emission peak at 560 nm), such as the WR (WRvFire) or International Health Department J (IHD-J-Luc) strains via intranasal (IN) route. Following infection, mice are observed for lethality and for weight loss and bioluminescence is recorded daily or as specified following administration of D-luciferin substrate via IP route each time prior to imaging. The recorded bioluminescence within ROI (as described above in Sect. 9.1.3) is converted into numerical values of photon fluxes using Living Image 3.2 software (PerkinElmer Inc., Hopkinton, MA, USA) and is analyzed using a panel of statistical tools. This chapter describes four experiments that illustrate the imaging approach we have employed combined with various types of statistical analyses that can be applied to understand how bioluminescence data can answer pharmacology questions which depend on the type of treatment and the scientific question one is trying to resolve.

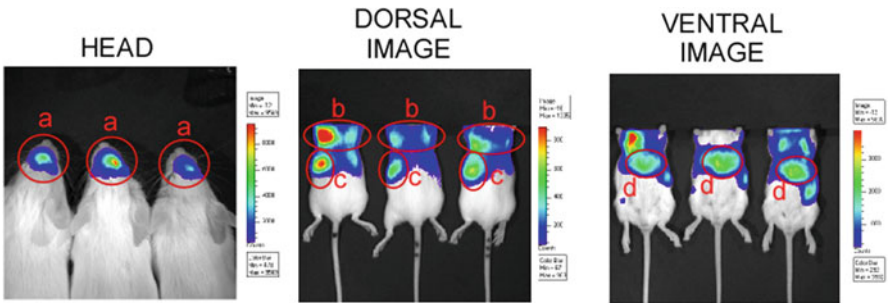

Fig. 9.1 Images of 5-week-old BALB/c mice infected with WRvFire VACV. Representative images of the heads (*left*), ventral torso (*center*), and dorsal torso (*right*) of mice infected with 10^5 pfu of WRvFire via the intranasal route are shown. Strong bioluminescence signals were noted in the nasal cavity (**a**), lungs (**b**), spleen (**c**), and liver (**d**). *Circles* mark the regions of interest (ROI) used to calculate total fluxes for subsequent analyses

9.5.1 Usage of Bioluminescence Recordings to Predict Lethality

The objective of the first approach was to determine whether a bioluminescence marker recorded using the IVIS 50 bioluminescence imaging instrument (PerkinElmer, Hopkinton, MA) in selected organs of infected mice (i.e., nasal cavity, lungs, spleen, and liver as shown in Fig. 9.1) was predictive of infection outcome, lethality versus survival. To answer this question, normal BALB/c mice (nine per group) were immunized with a licensed Dryvax vaccine that is considered a "gold standard" due to the long-lasting immune response in humans (Amanna et al. 2006; Hammarlund et al. 2003) or received PBS (control group) via IP injection, and 2 weeks later were challenged with a lethal dose of WRvFire (10 LD_{50}) via the IN route (Fig. 9.2) (Zaitseva et al. 2009). Control mice succumbed within 1 week post infection (p.i.), while all mice that received Dryvax survived (Fig. 9.2a, closed circles and open squares, respectively). In Dryvax-vaccinated mice, bioluminescence (photon flux) was not detected in the spleens and livers (data not shown). In the nasal cavity and lungs, photon fluxes were recorded on day 1 p.i., and were similar between control mice (closed circles) and immunized mice (open squares) (Fig. 9.2b, c, respectively).[1] Starting from days 3 to 4 p.i., photon fluxes were dramatically reduced in vaccinated but not in control mice suggesting that strong antiviral response induced by Dryvax vaccine protected mice from dissemination of WRvFire to the spleen and liver and rapidly cleared infection from the upper respiratory tract.

[1] Each curve represents specific wavelength photon fluxes recorded in one mouse on subsequent days.

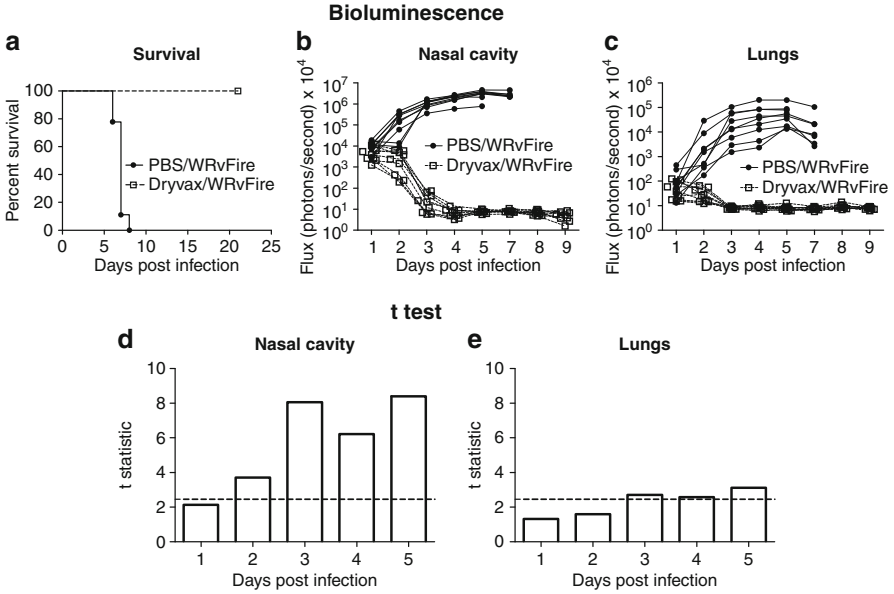

Fig. 9.2 Survival curves (**a**), bioluminescence in the nasal cavity (**b**), and lungs (**c**), and *t* statistics of the mean fluxes measured in the nasal cavity (**d**) and lungs (**e**) in mice that were challenged with WRvFire following immunization with Dryvax vaccine (on week 2). **b** and **c** illustrate the differences in the means of total fluxes between control animals (unimmunized, *closed circles*, $n=9$) and mice that were immunized with Dryvax vaccine (*open squares*, $n=9$) and survived challenge. **d** and **e** show significant differences in fluxes between Dryvax-vaccinated and control mice on days 2–5 in the nasal cavity and on days 3–5 for the lungs, $t \geq 2.12$ (shown as *dashed line*)

Mean photon fluxes were compared between control and immunized mice using *t* tests. Values of the *t* statistic above 2.12 (Fig. 9.2d, e, dashed lines) correspond to significant differences ($p<0.05$) for groups of nine mice. Calculated *t* values were above this critical value for the photon fluxes in the Dryvax-vaccinated mice on days 2–5 and 3–5 in the nasal cavity and lungs, respectively (Fig. 9.2d, e). These data showed that Dryvax-immunized mice all survived lethal challenge and had either no bioluminescence signal in internal organs or significantly lower signals in the upper respiratory track compared with control mice. Therefore, in this scenario, representing sterilizing immunity due to a potent vaccine, a direct comparison of means of photon fluxes using *t*-tests can be sufficient to support the efficacy of treatment.

9.5.2 Usage of Bioluminescence Recording to Predict Lethality When 100 % Effectiveness of Treatment Is Not Expected

To illustrate a situation when treatment protects only a proportion of animals or, in other words, only a proportion of animals "respond" to treatment with a desirable outcome, we employed a more suitable statistical approach. Two hundred (200) BALB/c mice

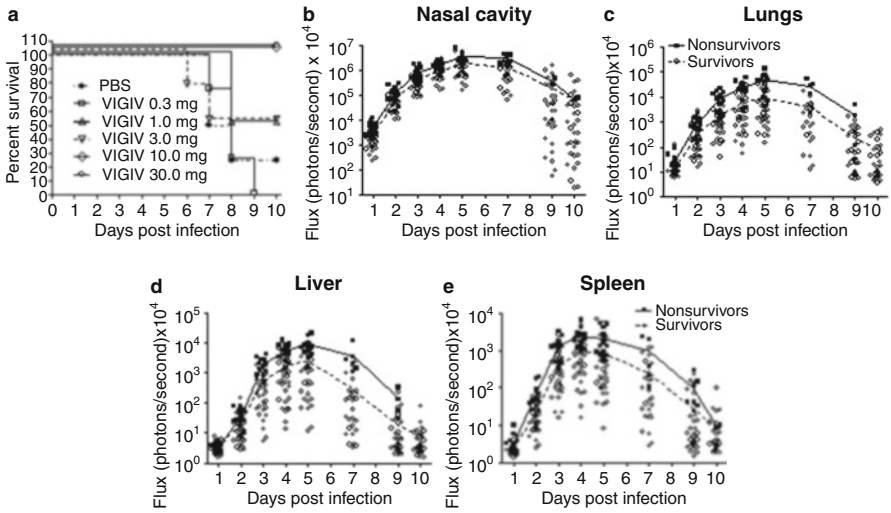

Fig. 9.3 Survival and bioluminescence in WRvFire-challenged mice that received pretreatment with VIGIV. Two hundred BALB/c mice (4–6 per group) received i.p. injections of VIGIV at doses 0.3, 1.0, 3.0, 10.0, and 30.0 mg per animal (or PBS in controls) 2 days before intranasal challenge. (**a**) The number of live mice was recorded each day and was used to calculate the percent survival. (**b–e**) The bioluminescence data per site/organ were obtained from six experiments. Daily fluxes in internal organs of surviving (*open circles*) and non-surviving mice (*closed circles*) of individual animals are shown. Total fluxes in the nasal cavity (**b**), lungs (**c**), liver (**d**), and spleen (**e**) were used to calculate means of total fluxes for surviving (*broken lines*) and non-surviving animals (*solid lines*). Total fluxes of 25 % of non-surviving (*closed symbols*) and 25 % surviving animals (*open symbols*) at each time point were randomly chosen using Excel's sampling for plotting in the graph

were treated IP with human Anti-Vaccinia Immunoglobulin for Intravenous use (VIGIV, Cangene Corporation, Winnipeg, Canada) at 5 doses ranging from 0.3 to 30 mg/animal or with PBS in controls, and 2 days later all mice were challenged with a lethal dose of WRvFire (Zaitseva et al. 2009). The study resulted in a true dose–response of none to 100 % of the lethally challenged mice to prophylaxis treatment with VIGIV (Fig. 9.3a). Bioluminescence recordings were acquired in all animals daily and mean photon fluxes in 4 organs of survived mice ($n=147$) and non-survived mice ($n=53$) were determined (Fig. 9.3b–e, closed vs. open symbols, respectively). Statistical analysis involved a *t* test of the means of fluxes recorded in individual mice. Although *t*-tests showed that mean fluxes were significantly different between surviving and non-surviving mice in all organs, some overlap in the signals was noted among the groups. These data prompted us to identify a statistical tool predictive of protection from lethality based on *threshold bioluminescence.*

Receiver operating characteristic (ROC) curve analysis is a graphical statistical tool that quantifies the ability of a prediction score to distinguish between "responders" and "nonresponders" by plotting *sensitivity* versus *1-specificity* for a binary classifier system as its discrimination threshold varies. As demonstrated in Fig. 9.4, four scenarios are possible for each predicted outcome: (1) bioluminescence in mice that did not survive could be above threshold (true positive, TP) or

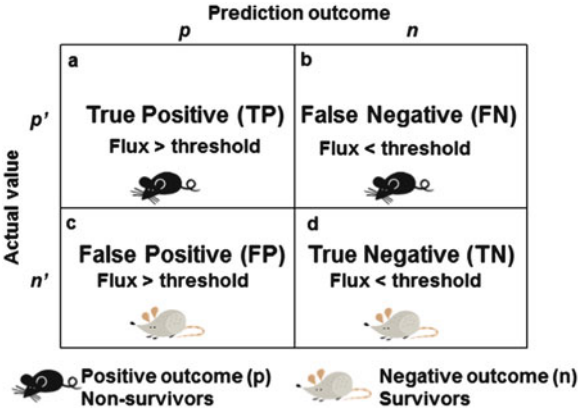

Fig. 9.4 *Confusion matrix* describing actual and predicted lethality in BALB/c mice challenged with WRvFire after they received prophylaxis treatment with VIGIV. This table explains the possible outcomes of a binary prediction rule. Study animals fall into four possible categories: (**a**) True positives are mice that died (positive outcome, p′) and were correctly predicted to die based on the levels of bioluminescence above threshold (positive prediction, p); (**b**) false negatives are mice that died (p′) and were incorrectly predicted to survive (negative prediction, n) based on the levels of bioluminescence below threshold; (**c**) false positives are mice that survived (negative outcome, n′) and were incorrectly predicted to die (p); (**d**) true negatives are mice that survived (n′) and were correctly predicted to survive (n)

(2) below threshold (false negative, FN); similarly, (3) mice that survived could exhibit signal below threshold (true negative, TN) or (4) exhibit signal above threshold (false positive, FP). Based on this assumption, the *sensitivity* of a prediction threshold is calculated as the ratio of the number of mice correctly predicted to die based on the level of bioluminescence to the number of all mice that died, TP/(TP+FN), and *specificity* is calculated as the ratio of the number of mice that had signal below threshold and survived to the total number of survived mice, TN/(FP+TN). Knowing the lethality/survival outcome for all 200 animals, sensitivity was plotted against 1-specificity for each value of recorded flux to calculate area under the ROC curve (AUC) for predictions based on bioluminescence levels in each of the four organs and for each of the days 1–5 following VACV challenge. The 5-day time frame for AUC analysis was selected based on the observation that all mice were alive during the first 5 days p.i. (Fig. 9.3a). Thus, bioluminescence recordings obtained during the first 5 days could be compared between mice that eventually survived or did not survive the challenge (Fig. 9.5). The highest AUC of 0.88–0.91 and of 0.91–0.87 were calculated for days 3–5 in the liver and spleen, respectively, suggesting that measurements of bioluminescence in these organs at these time points predicted lethality with greatest accuracy (Fig. 9.5). This approach showed that ROC analysis of the bioluminescence recordings can serve as a useful prediction tool when 100 % effectiveness of the treatment is not expected.

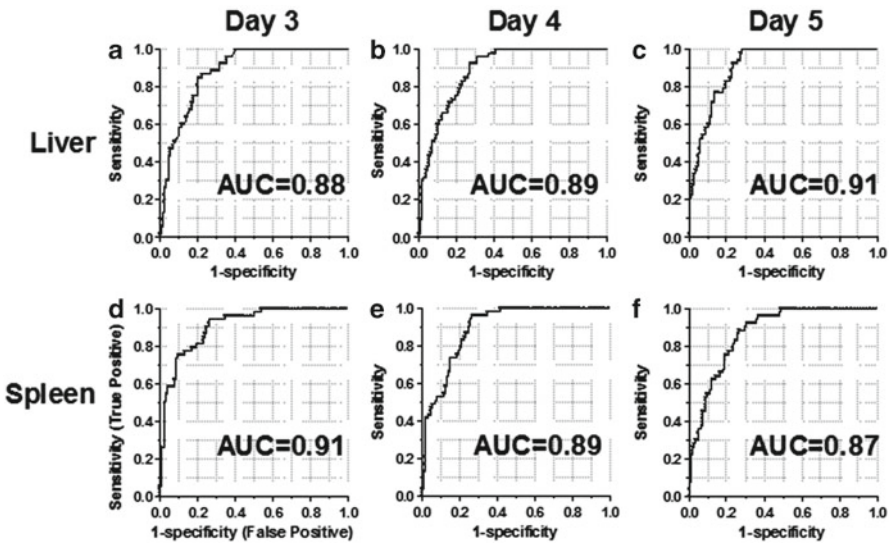

Fig. 9.5 ROC analyses of total fluxes in surviving and non-surviving mice. AUC values for liver (**a–c**) and spleen (**d–f**) were computed on days 3, 4, and 5 using fluxes recorded in mice described in the legend of Fig. 9.3 on days 1–5 post infection. This figure illustrates graphic format of ROC analysis

9.5.3 Usage of Bioluminescence to Assess the Effects of Doses on the Outcome of Treatment

In the third scenario, we used *t*-tests to determine the effects of treatment doses on viral loads (as assayed by recorded bioluminescence) in a given organ on a given day post challenge (Fig. 9.6). Groups of BALB/c mice (12 animals per group) received VIGIV at 30 mg/animal (open triangles) or 3 mg/animal (open squares) or PBS in controls (closed circles) 2 days prior to lethal challenge with WRvFire (Fig. 9.6a–e) or with IHD-J-Luc VACV (Fig. 9.6f–j) (Zaitseva et al. 2011). All control mice died within 1 week (Fig. 9.6a, f, closed circles); VIGIV at 30 mg protected 100 % of animals in both infections (Fig. 9.6a, f, open triangles). However, VIGIV at 3 mg protected only 33 and 17 % of mice infected with WRvFire or with IHD-J-Luc, respectively (Fig. 9.6a, f, open squares). Bioluminescence was recorded in all animals daily and mean photon fluxes per organ per group were calculated and plotted. As can be seen in Fig. 9.6b–e and g–j, viral loads in all survived mice returned to baseline levels on days 10–14.

To determine if treatment with the two doses of VIGIV significantly affected viral loads in each organ, mean photon fluxes were compared between control and treated mice using *t*-tests (*t* critical value = 2.07 for groups of 12 mice; dotted lines in Fig. 9.6k–r). In the nasal cavity, there were no significant differences in viral

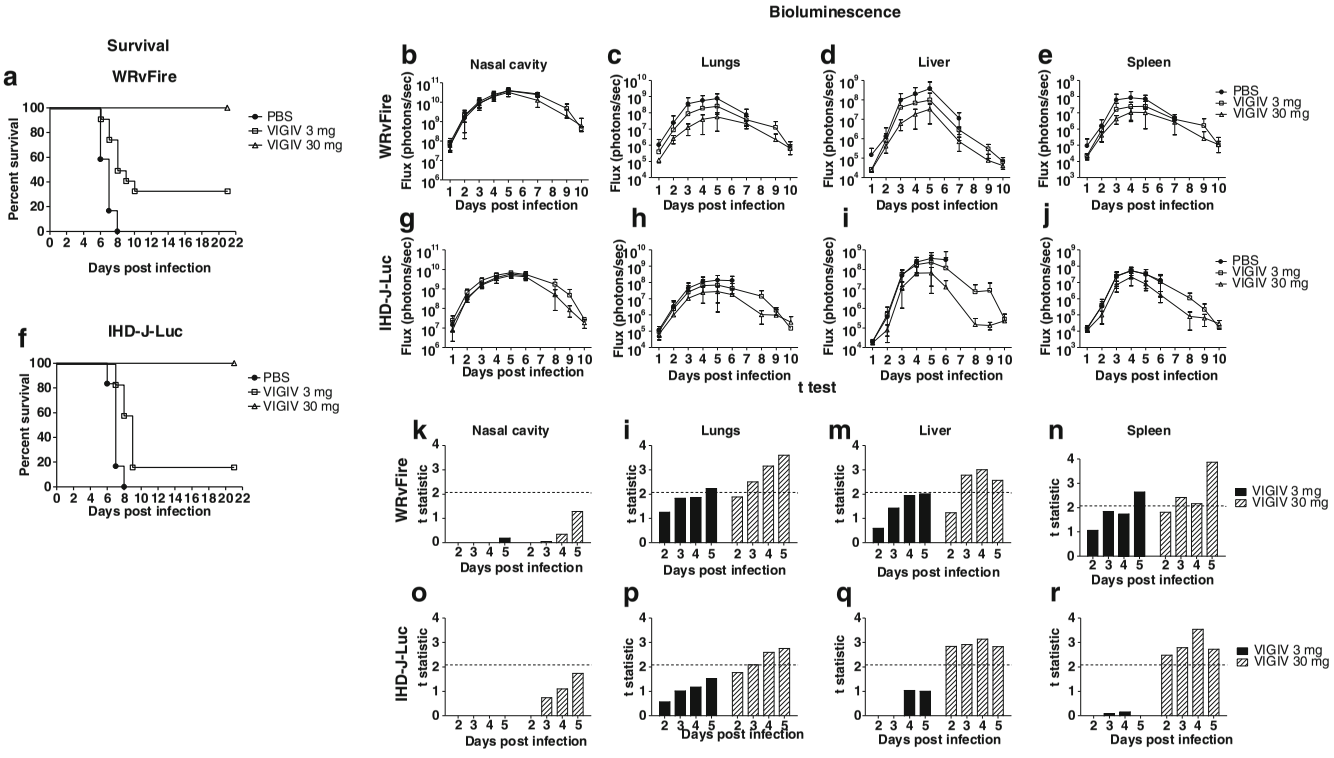

Fig. 9.6 (**a**–**f**) BALB/c mice (12 animals per group) received VIGIV at 30 mg/animal (*open triangles*) or 3 mg/animal (*open squares*) or PBS in controls (*closed circles*) 2 days prior to lethal challenge with WRvFire. Lethality Kaplan–Meier survival curves. (**b**–**e**) and (**g**–**j**). Bioluminescence, and *t*-tests of means of fluxes in mice that were treated with VIGIV and challenged with WRvFire or IHD-J-Luc VACV. Six BALB/c mice per group received PBS (*closed circles*) or VIGIV at 30 mg/animal (*open triangles*) or at 3 mg/animal (*open squares*) and were challenged 2 days later with WRvFre (**a**–**e**) or with IHD-J-Luc (**f**–**j**). Bioluminescence was recorded and used to calculate mean fluxes ± STDEV in the nasal cavity (**b**, **g**), lungs (**c**, **h**), liver (**d**, **i**), and spleen (**e**, **j**). (**k**–**n**, **o**–**r**) Significant differences (*t* values above *dotted lines*) between fluxes recorded in control mice and mice that received 3 mg (*solid bars*) or 30 mg (*hatched bars*) of VIGIV per animal and that were challenged with WRvFire or with IHD-J-Luc are shown in panels **k**–**n** and **o**–**r**, respectively. This figure illustrates a relationship between protection from lethality conferred by 30 mg of VIGIV and significant reduction in viral loads in three organs (lungs, liver, and spleen) on three consecutive days, days 3, 4, and 5

loads between VIGIV-treated and control mice for either dose of VIGIV at any time points in either virus infection (Fig. 9.6 panels k and o). In the lungs, liver, and spleen, viral loads were significantly different between mice that were treated with a 30 mg dose but not with 3 mg dose of VIGIV and control mice (hatched and solid bars, respectively), between days 3 and 5 (panels i–n in WRvFire infection and panels p–r in IHD-J-Luc infection). These statistical analyses demonstrated a correlation between protection from lethality and significant reduction in viral loads in 3 organs (lungs, liver, and spleen) on 3 consecutive days (days 3–5 p.i.). It also showed that significant reduction in viral loads for only 1 or 2 days in any individual site, as shown for VIGIV at 3 mg, did not confer protection from lethality (Fig. 9.6 panels i, m, and n, filled bars). Furthermore, these analyses underscore the conclusion that measurements of bioluminescence at a single time point may not be sufficient for assessing the efficacy of treatment. Accurate prediction of drug effectiveness might be improved by bioimaging at multiple time points and in several key organs as illustrated below.

9.5.4 Calculation of Areas Under the Flux Curve (AUC) for the Entire Survival Period Post Challenge

In the fourth scenario, we employed analysis of bioluminescence in infected mice to relate the efficacy of post-challenge treatment to the day of treatment initiation. In this approach, BALB/c mice were infected with IHD-J-Luc VACV and were treated IP with the antiviral drug Cidofovir (100 mg/kg dose) at 1, 2, 3, or 4 days post challenge. Controls were administered PBS (Fig. 9.7). Cidofovir is approved for treatment of cytomegalovirus (CMV) retinitis in AIDS patients and is the only antiviral compound approved by CDC for postexposure treatment of smallpox virus infections; see the Web site: http://www.bt.cdc.gov/agent/smallpox/vaccination/mgmt-adv-reactions.asp. All no-treatment control mice succumbed within 1 week (Fig. 9.7a, black curves), while all mice that received Cidofovir starting on day 1, 2, or 3 p.i. survived (Fig. 9.7a, red, blue, and green curves, respectively). Five out of six mice (83 %) survived when treatment was initiated on day 4 p.i. (Fig. 9.7a, purple curves). Mice were subjected to bioimaging daily and the recorded bioluminescence from individual mice was used to calculate and to plot mean photon fluxes for groups of six mice per group in the nasal cavity, lungs, liver, and spleen (Fig. 9.7b–e). As depicted in Fig. 9.7b–e, the bioluminescence signal returned to background levels in the lungs, liver, and spleen in all survived animals by day 14 p.i. and in the nasal cavity by day 30 (data not shown). Yet, there were clear differences in shapes of flux curves between groups suggesting that the delay in initiation of Cidofovir treatment post challenge might affect the kinetics of virus clearance.

To determine which delay in Cidofovir treatment significantly affected IHDJ-Luc viral loads, areas under the flux curves (AUC) were calculated for days 1–6 for all mice. These AUCs reflect the combined fluxes per organ per mouse representing cumulative viral loads during the observation period when all animals were still

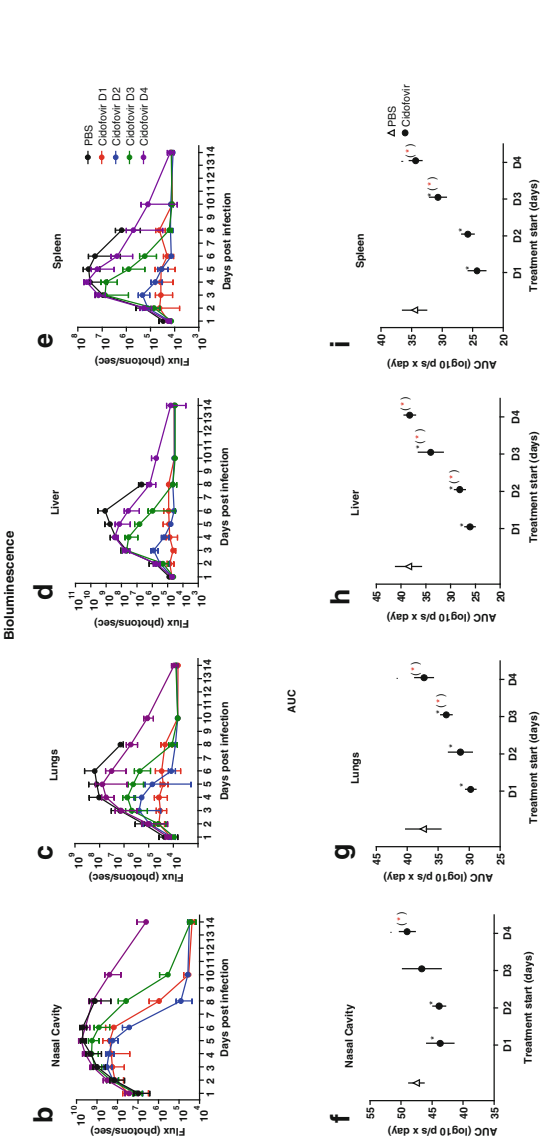

Fig. 9.7 (**a**–**i**) Survival curves, bioluminescence, and *t*-tests of the AUC for fluxes recorded in mice that received Cidofovir post challenge. BALB/c mice were infected with IHD-J-Luc and were treated with Cidofovir at 100 mg/kg on day 1 (*red curves*), day 2 (*blue curves*), day 3 (*green curves*), or day 4 (*purple curves*), or with PBS on day 1 (*black curves*) p.i. Mice were observed for survival (**a**) and bioluminescence was recorded and used to calculate mean fluxes ± STDEV in the nasal cavity (**b**), lungs (**c**), liver (**d**), and spleen (**e**). AUC for fluxes recorded between days 1 and 6 in the nasal cavity (**f**), lungs (**g**), liver (**h**), and spleen (**i**) in control mice (*open triangles*) and in mice that received Cidofovir at days 1, 2, 3, or 4 were computed and comparisons were made with *t*-tests. Black asterisks denote significant differences in AUC (viral loads) between control mice (*open triangles*) and mice that received Cidofovir (*closed circles*); asterisks in parenthesis denote significant differences in AUC (viral loads) between mice that received Cidofovir on day 1 versus day 2, 3, or 4 ($p \leq 0.05$)

alive (days 1–6 p.i.). Mean AUCs for groups of mice were compared with *t*-tests. AUCs in the lungs, liver, and spleen were significantly different between untreated control mice (open triangles) and mice that received Cidofovir (closed circles) starting on day 1, 2, or 3 post challenge (Fig. 9.7g–i). In the nasal cavity, AUCs were significantly different between control and treated mice only when treatment was delayed for 1 or 2 days (Fig. 9.7f). Although treatment initiated on day 4 p.i. rescued 83 % of animals from lethality, it failed to significantly reduce AUC (as a depiction of viral loads) compared to control mice in any of the organs that exhibited bioluminescence. We also compared AUCs between treatment groups only and found significant differences in the AUC in mice that initiated Cidofovir treatment on day 1 compared with day 3 or 4 (in the lungs, spleen, and liver). There were no significant differences in lethality or in viral loads if Cidofovir was administered on day 1 or 2 p.i. However, longer delay of ≥ 3 days was found to be protective from lethality, but was less efficient in reducing viral loads in all four organs.

9.6 Conclusions

Altogether our data showed that the use of bioluminescence imaging as a quantitative tool for assessing replication and dissemination of VACV in live mice, combined with a set of statistical tools (the *t* test, AUC, and ROC analysis), allowed us to (1) conserve significantly in the number of animals needed, (2) monitor dissemination of the virus within the same host over time including assessment of replication in hard-to-access anatomical sites within reasonable limits of detection, (3) generate models for prediction of lethality, and (4) gain insight regarding the effects of antiviral treatments on virus distribution over time and the quantitation of organ burdens (proportional to light intensity) as it relates to protection from lethality. Dissemination to the skin (i.e., pox formation) was also monitored. The bioimaging provides additional important information on the drug–pathogen–host interactions that correlate with organ pathology and between-host transmissibility that cannot be fully appreciated with the traditional models.

References

Amanna IJ, Slifka MK, Crotty S (2006) Immunity and immunological memory following smallpox vaccination. Immunol Rev 211:320–337

Andreu N, Zelmer A, Fletcher T, Elkington PT, Ward TH, Ripoll J, Parish T, Bancroft GJ, Schaible U, Robertson BD, Wiles S (2010) Optimisation of bioluminescent reporters for use with mycobacteria. PLoS One 5:e10777

Baker RO, Bray M, Huggins JW (2003) Potential antiviral therapeutics for smallpox, monkeypox and other orthopoxvirus infections. Antiviral Res 57:13–23

Belongia EA, Naleway AL (2003) Smallpox vaccine: the good, the bad, and the ugly. Clin Med Res 1:87–92

Berger F, Paulmurugan R, Bhaumik S, Gambhir SS (2008) Uptake kinetics and biodistribution of 14C-D-luciferin–a radiolabeled substrate for the firefly luciferase catalyzed bioluminescence reaction: impact on bioluminescence based reporter gene imaging. Eur J Nucl Med Mol Imaging 35:2275–2285

Bernthal NM, Stavrakis AI, Billi F, Cho JS, Kremen TJ, Simon SI, Cheung AL, Finerman GA, Lieberman JR, Adams JS, Miller LS (2010) A mouse model of post-arthroplasty Staphylococcus aureus joint infection to evaluate in vivo the efficacy of antimicrobial implant coatings. PLoS One 5:e12580

Bina XR, Miller MA, Bina JE (2010) Construction of a bioluminescence reporter plasmid for Francisella tularensis. Plasmid 64:156–161

Burke CW, Mason JN, Surman SL, Jones BG, Dalloneau E, Hurwitz JL, Russell CJ (2011) Illumination of parainfluenza virus infection and transmission in living animals reveals a tissue-specific dichotomy. PLoS Pathog 7:e1002134

Collins JW, Akin AR, Kosta A, Zhang N, Tangney M, Francis KP, Frankel G (2012) Pre-treatment with Bifidobacterium breve UCC2003 modulates Citrobacter rodentium-induced colonic inflammation and organ specificity. Microbiology 158:2826–2834

Contag CH, Bachmann MH (2002) Advances in in vivo bioluminescence imaging of gene expression. Annu Rev Biomed Eng 4:235–260

Contag CH, Contag PR, Mullins JI, Spilman SD, Stevenson DK, Benaron DA (1995) Photonic detection of bacterial pathogens in living hosts. Mol Microbiol 18:593–603

Cook SH, Griffin DE (2003) Luciferase imaging of a neurotropic viral infection in intact animals. J Virol 77:5333–5338

Doyle TC, Nawotka KA, Kawahara CB, Francis KP, Contag PR (2006) Visualizing fungal infections in living mice using bioluminescent pathogenic Candida albicans strains transformed with the firefly luciferase gene. Microb Pathog 40:82–90

Edghill-Smith Y, Golding H, Manischewitz J, King LR, Scott D, Bray M, Nalca A, Hooper JW, Whitehouse CA, Schmitz JE, Reimann KA, Franchini G (2005) Smallpox vaccine-induced antibodies are necessary and sufficient for protection against monkeypox virus. Nat Med 11:740–747

Enjalbert B, Rachini A, Vediyappan G, Pietrella D, Spaccapelo R, Vecchiarelli A, Brown AJ, d'Enfert C (2009) A multifunctional, synthetic Gaussia princeps luciferase reporter for live imaging of Candida albicans infections. Infect Immun 77:4847–4858

Fenner F, Henderson DA, Arita I, Jezek Z, Ladnyi ID (1988) Smallpox and its iradication. World Health Organization, Geneva, Switzerland

Francis KP, Joh D, Bellinger-Kawahara C, Hawkinson MJ, Purchio TF, Contag PR (2000) Monitoring bioluminescent Staphylococcus aureus infections in living mice using a novel luxABCDE construct. Infect Immun 68:3594–3600

Francis KP, Yu J, Bellinger-Kawahara C, Joh D, Hawkinson MJ, Xiao G, Purchio TF, Caparon MG, Lipsitch M, Contag PR (2001) Visualizing pneumococcal infections in the lungs of live mice using bioluminescent Streptococcus pneumoniae transformed with a novel gram-positive lux transposon. Infect Immun 69:3350–3358

Glomski IJ, Piris-Gimenez A, Huerre M, Mock M, Goossens PL (2007) Primary involvement of pharynx and peyer's patch in inhalational and intestinal anthrax. PLoS Pathog 3:e76

Gould SJ, Subramani S (1988) Firefly luciferase as a tool in molecular and cell biology. Anal Biochem 175:5–13

Hammarlund E, Lewis MW, Hansen SG, Strelow LI, Nelson JA, Sexton GJ, Hanifin JM, Slifka MK (2003) Duration of antiviral immunity after smallpox vaccination. Nat Med 9:1131–1137

Henderson DA, Inglesby TV, Bartlett JG, Ascher MS, Eitzen E, Jahrling PB, Hauer J, Layton M, McDade J, Osterholm MT, O'Toole T, Parker G, Perl T, Russell PK, Tonat K (1999) Smallpox as a biological weapon: medical and public health management. Working Group on Civilian Biodefense. JAMA 281:2127–2137

Hooper JW, Thompson E, Wilhelmsen C, Zimmerman M, Ichou MA, Steffen SE, Schmaljohn CS, Schmaljohn AL, Jahrling PB (2004) Smallpox DNA vaccine protects nonhuman primates against lethal monkeypox. J Virol 78:4433–4443

Hutchens MA, Luker KE, Sonstein J, Nunez G, Curtis JL, Luker GD (2008) Protective effect of Toll-like receptor 4 in pulmonary vaccinia infection. PLoS Pathog 4:e1000153

Kadurugamuwa JL, Sin LV, Yu J, Francis KP, Kimura R, Purchio T, Contag PR (2003) Rapid direct method for monitoring antibiotics in a mouse model of bacterial biofilm infection. Antimicrob Agents Chemother 47:3130–3137

Krug A, Luker GD, Barchet W, Leib DA, Akira S, Colonna M (2004) Herpes simplex virus type 1 activates murine natural interferon-producing cells through toll-like receptor 9. Blood 103: 1433–1437

Lang T, Goyard S, Lebastard M, Milon G (2005) Bioluminescent Leishmania expressing luciferase for rapid and high throughput screening of drugs acting on amastigote-harbouring macrophages and for quantitative real-time monitoring of parasitism features in living mice. Cell Microbiol 7:383–392

Lee KH, Byun SS, Paik JY, Lee SY, Song SH, Choe YS, Kim BT (2003) Cell uptake and tissue distribution of radioiodine labelled D-luciferin: implications for luciferase based gene imaging. Nucl Med Commun 24:1003–1009

Lin MZ, McKeown MR, Ng HL, Aguilera TA, Shaner NC, Campbell RE, Adams SR, Gross LA, Ma W, Alber T, Tsien RY (2009) Autofluorescent proteins with excitation in the optical window for intravital imaging in mammals. Chem Biol 16:1169–1179

Luker GD, Bardill JP, Prior JL, Pica CM, Piwnica-Worms D, Leib DA (2002) Noninvasive bioluminescence imaging of herpes simplex virus type 1 infection and therapy in living mice. J Virol 76:12149–12161

Luker GD, Prior JL, Song J, Pica CM, Leib DA (2003) Bioluminescence imaging reveals systemic dissemination of herpes simplex virus type 1 in the absence of interferon receptors. J Virol 77:11082–11093

Luker KE, Hutchens M, Schultz T, Pekosz A, Luker GD (2005) Bioluminescence imaging of vaccinia virus: effects of interferon on viral replication and spread. Virology 341:284–300

Luker KE, Luker GD (2008) Applications of bioluminescence imaging to antiviral research and therapy: multiple luciferase enzymes and quantitation. Antiviral Res 78:179–187

Morin CE, Kaper JB (2009) Use of stabilized luciferase-expressing plasmids to examine in vivo-induced promoters in the Vibrio cholerae vaccine strain CVD 103-HgR. FEMS Immunol Med Microbiol 57:69–79

Neyts J, De Clercq E (2003) Therapy and short-term prophylaxis of poxvirus infections: historical background and perspectives. Antiviral Res 57:25–33

Nham T, Filali S, Danne C, Derbise A, Carniel E (2012) Imaging of bubonic plague dynamics by in vivo tracking of bioluminescent Yersinia pestis. PLoS One 7:e34714

Panchanathan V, Chaudhri G, Karupiah G (2007) Correlates of protective immunity in poxvirus infection: where does antibody stand? Immunol Cell Biol 86:80–86

Paroo Z, Bollinger RA, Braasch DA, Richer E, Corey DR, Antich PP, Mason RP (2004) Validating bioluminescence imaging as a high-throughput, quantitative modality for assessing tumor burden. Mol Imaging 3:117–124

Patterson M, Poussard A, Taylor K, Seregin A, Smith J, Peng BH, Walker A, Linde J, Salazar M, Paessler S (2011) Rapid, non-invasive imaging of alphaviral brain infection: reducing animal numbers and morbidity to identify efficacy of potential vaccines and antivirals. Vaccine 29:9345–9351

Rhee KJ, Cheng H, Harris A, Morin C, Kaper JB, Hecht G (2011) Determination of spatial and temporal colonization of enteropathogenic E. coli and enterohemorrhagic E. coli in mice using bioluminescent in vivo imaging. Gut Microbes 2:34–41

Rimoin AW, Mulembakani PM, Johnston SC, Lloyd Smith JO, Kisalu NK, Kinkela TL, Blumberg S, Thomassen HA, Pike BL, Fair JN, Wolfe ND, Shongo RL, Graham BS, Formenty P, Okitolonda E, Hensley LE, Meyer H, Wright LL, Muyembe JJ (2010) Major increase in human monkeypox incidence 30 years after smallpox vaccination campaigns cease in the Democratic Republic of Congo. Proc Natl Acad Sci USA 107:16262–16267

Rodriguez JF, Rodriguez D, Rodriguez JR, McGowan EB, Esteban M (1988) Expression of the firefly luciferase gene in vaccinia virus: a highly sensitive gene marker to follow virus dissemination in tissues of infected animals. Proc Natl Acad Sci USA 85:1667–1671

Roy G, Dumas C, Sereno D, Wu Y, Singh AK, Tremblay MJ, Ouellette M, Olivier M, Papadopoulou B (2000) Episomal and stable expression of the luciferase reporter gene for quantifying Leishmania spp. infections in macrophages and in animal models. Mol Biochem Parasitol 110:195–206

Saeij JP, Boyle JP, Grigg ME, Arrizabalaga G, Boothroyd JC (2005) Bioluminescence imaging of Toxoplasma gondii infection in living mice reveals dramatic differences between strains. Infect Immun 73:695–702

Schoggins JW, Dorner M, Feulner M, Imanaka N, Murphy MY, Ploss A, Rice CM (2012) Dengue reporter viruses reveal viral dynamics in interferon receptor-deficient mice and sensitivity to interferon effectors in vitro. Proc Natl Acad Sci USA 109:14610–14615

Sha J, Rosenzweig JA, Kirtley ML, van Lier CJ, Fitts EC, Kozlova EV, Erova TE, Tiner BL, Chopra AK (2013) A non-invasive in vivo imaging system to study dissemination of bioluminescent Yersinia pestis CO92 in a mouse model of pneumonic plague. Microb Pathog 55:39–50

Sweeney TJ, Mailander V, Tucker AA, Olomu AB, Zhang W, Cao Y, Negrin RS, Contag CH (1999) Visualizing the kinetics of tumor-cell clearance in living animals. Proc Natl Acad Sci USA 96:12044–12049

Troy T, Jekic-McMullen D, Sambucetti L, Rice B (2004) Quantitative comparison of the sensitivity of detection of fluorescent and bioluminescent reporters in animal models. Mol Imaging 3:9–23

Whitley RJ (2003) Smallpox: a potential agent of bioterrorism. Antiviral Res 57:7–12

Xiong YQ, Willard J, Kadurugamuwa JL, Yu J, Francis KP, Bayer AS (2005) Real-time in vivo bioluminescent imaging for evaluating the efficacy of antibiotics in a rat Staphylococcus aureus endocarditis model. Antimicrob Agents Chemother 49:380–387

Zaitseva M, Kapnick SM, Meseda CA, Shotwell E, King LR, Manischewitz J, Scott J, Kodihalli S, Merchlinsky M, Nielsen H, Lantto J, Weir JP, Golding H (2011) Passive immunotherapies protect WRvFire and IHD-J-Luc vaccinia virus-infected mice from lethality by reducing viral loads in the upper respiratory tract and internal organs. J Virol 85:9147–9158

Zaitseva M, Kapnick SM, Scott J, King LR, Manischewitz J, Sirota L, Kodihalli S, Golding H (2009) Application of bioluminescence imaging to the prediction of lethality in vaccinia virus-infected mice. J Virol 83:10437–10447

Zhang Y, Pullambhatla M, Laterra J, Pomper MG (2012) Influence of bioluminescence imaging dynamics by D-luciferin uptake and efflux mechanisms. Mol Imaging 11:499–506